Available online at www.sciencedirect.com
ScienceDirect
Biochimica et Biophysica Acta 1778 (2008) 97–104
Biochimica et Biophysica Acta BBA
www.elsevier.com/locate/bbamem

Using ^{31}P MAS NMR to monitor a gel phase thermal disorder transition in sphingomyelin/cholesterol bilayers

Alison L. Costello, Todd M. Alam *

Department of Nanostructured and Electronic Materials, Sandia National Laboratories, Albuquerque, NM 87185-0886, USA

Received 5 June 2007; received in revised form 2 August 2007; accepted 31 August 2007
Available online 12 September 2007

Abstract

The impact of low cholesterol concentrations on an egg sphingomyelin bilayer is investigated using ^{31}P magic angle spinning (MAS) NMR spectroscopy. The magnitude of the isotropic ^{31}P MAS NMR line width is used to monitor the main gel to liquid crystalline phase transition, along with a unique gel phase pretransition. In addition, the ^{31}P chemical shift anisotropy (CSA) and spin–spin relaxation times (T_2), along with the effects of spinning speed, proton decoupling and magnetic field strength, are reported. The variation of this unique gel phase thermal pretransition with the inclusion of 5 through 21 mol% cholesterol is presented and discussed.

Keywords: Solid-state nuclear magnetic resonance; Sphingomyelin bilayer; Magic-angle spinning; Phase transition; Cholesterol; Gel phase

1. Introduction

The aggregation of saturated phospholipids and cholesterol in biomembranes to form lipid rafts [1,2] has generated considerable interest due to their proposed role in cellular processes, e.g., protein trafficking, signal transduction [3], and possible toxin and virus entry sites [4]. Previous studies show that the incorporation of cholesterol into the lipid bilayer broadens and lowers the main gel to liquid crystalline phase transition temperature (T_m) [5–7], decreases (increases) the lipid hydrocarbon chain ordering below (above) T_m [8,9], decreases the acyl chain tilt angle in the gel phase [10], and diminishes/eliminates the gel phase pretransition prior to T_m [7]. Below T_m, the addition of cholesterol can lead to the formation of a coexisting two-phase region involving the low cholesterol content solid-ordered (s_o) phase and the high cholesterol content liquid-ordered (l_o) phase [11], while above T_m a two-phase region involving the low cholesterol content liquid-disordered (l_d) phase and the high cholesterol content l_o phase results [11–15].

Cholesterol appears to have a higher affinity for sphingomyelin (SM) than for other phospholipids [9,16–21], most likely due to the distinct structural properties of SM. Sphingomyelin has a large phosphoryl choline headgroup that is well hydrated, allowing more favorable insertion of cholesterol and shielding for the hydrophobic cholesterol molecules [18,19,22–25]. The backbone and acyl chain regions of SM distinguish it from other lipids with the same headgroup (i.e., phosphatidylcholines, PCs) [16,24]. The sphingosine backbone consists of two H-bond donor groups (OH and NH group) and one H-bond acceptor group (carbonyl), compared to the glycerol backbone of PC which only has two carbonyl H-bond acceptors. The main SM-cholesterol interaction has been experimentally shown to occur between the NH group of SM and the OH group of cholesterol [26–28], a finding also supported by molecular dynamic simulations [9]. The hydrophobic acyl chain regions of SM and PC also have an important impact on chain packing effects. Natural SMs have a high degree of saturation in the acyl chain, resulting in stronger van der Waals interactions between SM and cholesterol. Naturally occurring PCs, on the other hand, have a high occurrence of unsaturation which weakens the PC–cholesterol interaction [6,17,18].

Until recently, only saturated phosphatidylcholines (e.g., DPPC) were known to form a rippled phase ($P_{\beta'}$), or pretransition phase. This rippled phase is intermediate to the motionally

Abbreviations: SM, sphingomyelin; PC, phosphatidylcholine; Chol, cholesterol; MAS NMR, magic-angle spinning nuclear magnetic resonance; DSC, differential scanning calorimetry; CSA, chemical shift anisotropy; FWHM, full width at half maximum

* Corresponding author. Tel.: +1 505 844 1225; fax: +1 505 844 2974.
E-mail address: tmalam@sandia.gov (T.M. Alam).

0005-2736/$ - see front matter © 2007 Elsevier B.V. All rights reserved.
doi:10.1016/j.bbamem.2007.08.031

restricted gel phase and the fluid liquid crystalline phase [29] and is characterized by a long-wavelength rippling of the bilayer and a swelling of the membrane [30]. In the past two decades, several reports of gel phase pretransitions in sphingomyelin bilayers have emerged. These pretransitions have been detected by differential scanning calorimetry [6,7,10,31–38], freeze-etch electron microscopy [35,36,39] and X-ray diffraction [10]. Several factors seem to effect the pretransition, including chain length, headgroup size, hydration, and possibly chain tilt [29]. In addition to these factors, the observation of a pretransition in SM appears to be dependent upon the type of SM sample. Thus far, pretransitions have been observed for brain SM [33,35,39], purified egg SM [7,37,38], synthetic C24 SM [6,10,34,36], synthetic C18 SM (D- and L-isomer) [32], synthetic C16 SM (D-isomer) [31], but not detected in racemic mixtures of SM [31,32] or unpurified egg SM. Interestingly, the X-ray diffraction data [6,10,40] for SM with long C24 chains indicate that other processes are occurring in the bilayer, e.g., chain interdigitation, resulting in the presence of another type of transition prior to the main transition. Thus, for SM, hydration, chain length, chain heterogeneity, and chirality seem to be factors in the occurrence and/or detection of a gel phase pretransition.

Previous NMR studies have revealed important information regarding the conformation and molecular dynamics in the SM bilayer. SM was shown to have similar headgroup motions and conformations as the glycerol-based phospholipids using ^{31}P NMR [41]. However, unlike PC, intermolecular H-bonding between SM amide groups and intramolecular H-bonding between the SM OH group and the phosphate headgroup was shown to be a significant factor in the rigidity of SM membranes using ^{1}H and ^{31}P NMR [42,43]. This result was further supported by molecular dynamic simulations [8,9,44–46]. In addition, restricted mobility in the gel phase was detected for both the SM headgroup and the acyl chains using ^{31}P and ^{13}C NMR, respectively. The mobility of the headgroup increased as cholesterol was added to the bilayer and resembled that seen in the liquid crystalline phase [20,47,48]. Multiple gel phases for SM have also been seen in ^{31}P NMR and ^{13}C NMR [49]. More recently, Holland et al. suggested that an additional gel phase transition was observable in the ^{31}P MAS NMR spectra of SM mixtures [48]. However, the appearance of this additional gel phase transition was quenched by the inclusion of 33% cholesterol. This paper continues this work with a ^{31}P MAS NMR analysis of the SM system at cholesterol concentrations below 33% to study the structural/dynamical changes occurring immediately prior to the main gel to liquid crystalline phase transition.

2. Materials and methods

2.1. Materials and sample preparation

Egg SM and Chol were obtained from Avanti Polar Lipids (Alabaster, AL) with no further purification. The SM contained the following acyl chain composition: 84% 16:0, 6% 18:0, 2% 20:0, 4% 22:0, 4% 24:0. Multilamellar vesicles (MLVs) of SM and SM/Chol were prepared in deionized water using five freeze–thaw cycles with a 2-min vortex time between each cycle. The freeze–thaw cycles were accomplished using a dry ice bath and a water bath set to 333 K (above the SM T_m). Hydrated samples contained 33 wt.% phospholipid with varying mol% of Chol. Lipid samples were transferred to 4 mm zirconia MAS rotors and sealed with kel-F inserts and caps. Sample volume for MAS experiments was ~50 μl of lipid MLV and ~100 μl of lipid MLV for static experiments. Samples were stored at −20 °C when not in use. The differential scanning calorimetry (DSC) spectra were obtained using a TA Instruments Q100 with a scan rate of 5 °C/min from 20 °C to 60 °C.

2.2. ^{31}P NMR spectroscopy

The NMR experiments were performed on either a Bruker Avance 600 at 242.9 MHz (14.1 T), or a Bruker Avance 400 at 162.0 MHz (9.4 T) using a 4-mm broad band MAS probe for both MAS and static conditions. A Bruker BVT 3000 temperature controller maintained the sample temperature to ±0.2 K for all experiments. Samples were allowed to equilibrate for 5 min at each temperature before acquisition. The ^{31}P MAS NMR experiments used a spinning speed of 2 kHz±1 Hz unless otherwise noted. An increase in sample temperature due to frictional heating from sample spinning is ~1 K for speeds ≤4 kHz and is ~3 K for a rotor speed of 6 kHz. Sample temperatures reported here have been calibrated using the method described previously [50]. The ^{31}P MAS NMR experiments utilized a single pulse Bloch decay with a 4.5 μs $\pi/2$ pulse, either without ^{1}H decoupling or with moderate (22.5 kHz) ^{1}H TPPM decoupling. Spin–spin relaxation times (T_2) were obtained under MAS conditions with a rotor synchronized spin-echo without ^{1}H decoupling. All MAS experiments utilized a 3-s recycle delay. Static ^{31}P NMR spectra were obtained using a Hahn spin-echo sequence ($\pi/2$–τ–π) with a $\pi/2$ pulse of 4.5 μs and an interpulse delay of 20 μs and moderate ^{1}H TPPM decoupling (22.5 kHz).

All ^{31}P chemical shift anisotropy (CSA) tensor fits were performed on the experimental spectra as previously described [48] using the DMFIT software package [51]. The anisotropic part of the CSA tensor is defined by

$$\Delta\sigma = \sigma_{33} - 1/2(\sigma_{22} + \sigma_{11}) \quad (1)$$

The asymmetry parameter of the CSA tensor is given by

$$\eta = \frac{(\sigma_{22} - \sigma_{11})}{(\sigma_{33} - \sigma_i)} \quad (2)$$

where σ_i is the isotropic chemical shift, and the principal tensor components (σ_{ii}) are ordered as follows: $|\sigma_{33}-\sigma_i| > |\sigma_{22}-\sigma_i| > |\sigma_{11}-\sigma_i|$. Above T_m the motionally averaged ^{31}P CSA tensor becomes an axially symmetric tensor leading to the anisotropy definition presented by Seelig

$$\Delta\sigma = \sigma_{\parallel} - \sigma_{\perp} = (3/2)(\sigma_{\parallel} - \sigma_i) \quad (3)$$

where $\sigma_{\parallel}$ is the low intensity shoulder ($\sigma_{\parallel}=\sigma_{33}$), and $\sigma_{\perp}$ is the high intensity shoulder ($\sigma_{\perp}=\sigma_{11}=\sigma_{22}$) [52]. The definition for $\Delta\sigma$ presented here differs from the definition of the anisotropy ($\Delta\delta$) defined by DMFIT [51] by a factor of 3/2

$$\Delta\delta = \sigma_{33} - \sigma_i \quad (4)$$

and has been taken into account for the $\Delta\sigma$ values reported here. The ^{31}P MAS NMR spectra, including all sideband resonances, were fit using a single spectral component in which $\Delta\sigma$ and η were allowed to vary. The line width was obtained by selectively fitting the isotropic resonance with a Lorentzian function.

3. Results and discussion

The ^{31}P MAS NMR spectra for pure SM MLVs below and above the main gel to liquid crystalline phase (L_α) transition temperature (T_m ~ 313 K [7,53,54]) are shown in Fig. 1. Below T_m the broad spinning sideband (SSB) manifold (Fig. 1a) reveals an asymmetric ^{31}P CSA tensor ($\Delta\sigma$=56.8 ppm, η=0.65) consistent with previously reported gel phase ^{31}P NMR spectra [48]. Above T_m, the ^{31}P MAS NMR spectrum (Fig. 1b) is axially symmetric (η=0) with a significantly smaller CSA value ($\Delta\sigma$= 44.5 ppm), consistent with a change in headgroup orientation

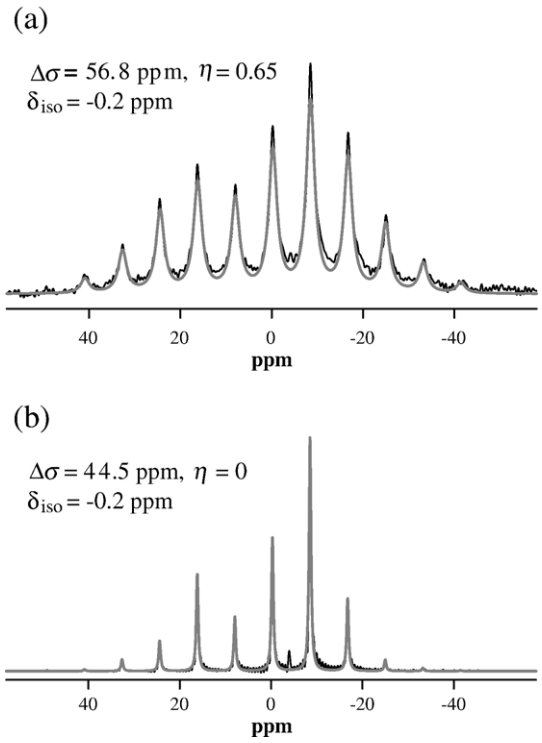

Fig. 1. The ^{31}P MAS NMR spectra (black lines) and simulations (gray lines) of SM bilayers (ν_r=2 kHz) at (a) 296 K (below T_m ~313 K) and (b) 318 K. The ^{31}P CSA parameters obtained from simulations are shown.

and/or the increased motional averaging of the headgroup in the liquid crystalline L_α phase, as previously discussed [47,48].

3.1. Variation of ^{31}P isotropic line width with temperature and cholesterol concentration

Previously, it was noted that the line widths of the isotropic resonance in the ^{31}P MAS NMR spectra of SM were temperature sensitive, and revealed some type of disordering or motional transition event (i.e., pretransition, gel → gel) occurring in the gel phase region (298 K to 310 K), prior to the main gel → L_α phase transition. The same type of ^{31}P MAS NMR line width variation can be seen in Fig. 2, where the isotropic line width of SM increases from ~328 Hz at 292 K to 530 Hz at 310 K, then drops dramatically to ~167 Hz following the main gel → L_α transition at ~312 K. The overall increase in FWHM for this SM gel phase transition is 202 Hz. This change is ~100 Hz smaller than previously reported [48] and is being attributed to the slight variability of lipid chain length distribution between different samples. Anecdotal evidence has shown that lot-to-lot variations of egg SM impact the magnitude of the observed temperature variations in the line width, such that for the work reported in this manuscript a single SM lot was employed for all samples.

It can also be seen in Fig. 2 that the addition of Chol impacts the extent of this ^{31}P MAS NMR line width variation just prior to the main gel → L_α transition. For example, increasing the Chol content to 5 mol% reduces the line width variation, with the maximum occurring at 306 K and an overall line width change reduced to 118 Hz (versus 202 Hz in pure SM). As the Chol content increases to 7.5 mol% this gel phase line width variation diminishes to ΔFWHM=50 Hz. For Chol concentrations >10 mol% this unique increase in the line width was not observed, instead revealing only a gradual decrease with increasing temperature throughout the gel phase.

A more detailed look at the effects of Chol on the ^{31}P MAS NMR line widths are shown in Fig. 3. Below T_m the line widths of SM bilayers with low Chol concentrations are broader compared to other SM/lipid mixtures (e.g., SM/DOPC, SM/DOPC/Chol [48]) and suggest either restricted phosphorus headgroup mobility and/or heterogeneity in the headgroup environment within the SM gel phase. With the addition of 5 or 7.5 mol% Chol to the SM bilayer, no changes in the line width are observed (Fig. 3b). At 10 mol% Chol, a 15.5% reduction in the line width occurs, and at 21 mol% Chol, an overall FWHM reduction of 34% was observed. SM with 33 mol% Chol (previous work) shows a slightly larger line width value (FWHM=270 Hz) [48] than the 21 mol% value (FWHM=236 Hz) reported, here but remains consistent with the overall trend. For cholesterol concentrations greater than 10 mol%, this reduction of the gel phase line width mirrors the reduction of the ^{31}P CSA values at higher cholesterol contents (see discussion below). Interestingly, below 10 mol% Chol no changes in the line width were observed at 296 K. Therefore, at 296 K (in the gel or s_o phase, and prior to the observation of the pretransition shown in Fig. 2) the inclusion of Chol at concentrations >10 mol% results in either an increased headgroup mobility or change in headgroup orientation, while below 10 mol% Chol changes in the headgroup dynamics on the timescale of the ^{31}P line width ($1/\Delta\delta_{iso}$) are not occurring. These results are consistent with previous studies in which increased headgroup mobility or changes in headgroup orientation were observed as cholesterol was added to the bilayer [47,48]. The phase diagram for *N*-palmitoyl-D-sphingomyelin (PSM)/Chol below T_m has been reported [11]. For intermediate Chol concentrations a two-phase region exists between the low cholesterol content s_o and l_o phases. The observed line width of 357 Hz (296 K) and 0 mol% Chol corresponds to the s_o phase, while the

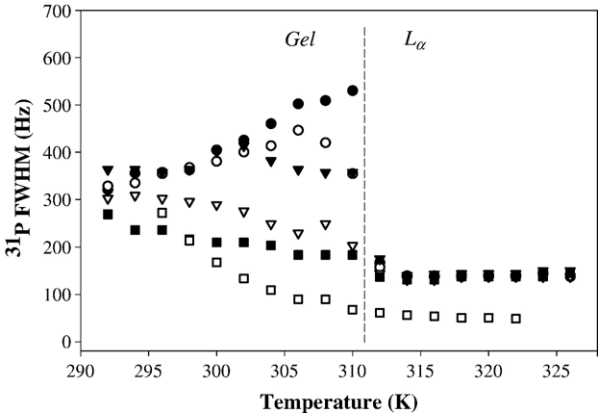

Fig. 2. The ^{31}P MAS NMR isotropic full width at half maximum (FWHM) line width as a function of temperature for (●) SM, (○) 5 mol% Chol, (▼) 7.5 mol% Chol, (▽) 10 mol% Chol, and (■) 21 mol% Chol. SM and 33 mol% Chol (□) is shown for comparison and is from a previous work [48].

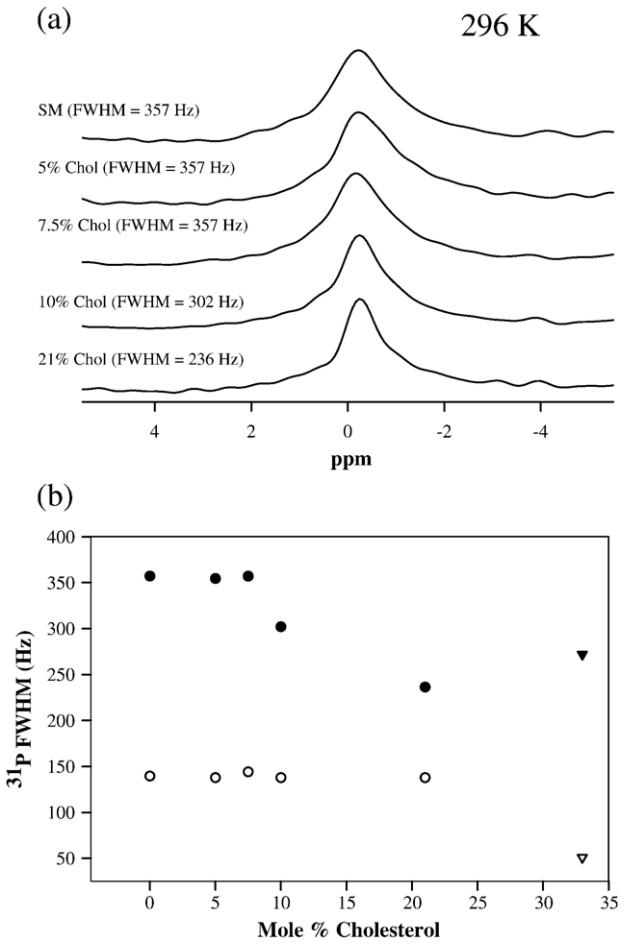

Fig. 3. The (a) ^{31}P MAS NMR isotropic chemical shift region of pure SM and SM with 5, 7.5, 10 and 21 mol% Chol at 296 K. The line width (b) as a function of Chol concentration at (●) 296 K and at (○) 318 K. SM and 33 mol% Chol at (▼) 296 K and (▽) 318 K from previous studies are also shown [48].

line width of 272 Hz of the 33 mol% Chol sample is characteristic of the l_o phase. The change in the ^{31}P MAS NMR line width between 10 and 20 mol% Chol may reflect the averaging within the mixed s_o+l_o phase, but is complicated by the presence of multiple gel phases [49].

Above T_m (318 K), the isotropic line width is ~140 Hz for all bilayers with concentrations up to 21 mol% Chol (Fig. 3b), after which a dramatic decrease in line width is seen at 33 mol% Chol. The phase diagram for SM/Chol above T_m also reveals the existence of a two-phase region, with the coexistence of the l_d and l_o phases [11,12,14,15]. At 0 mol% Chol the line width of 140 Hz (318 K) corresponds to the l_d phase while at 33 mol% Chol the line width of 51 Hz (318 K) represent the l_o phase. The lack of variation in the line width between 0 and 22 mol% Chol shows that the ^{31}P MAS NMR line width is not sensitive to the presence of the two-phase l_d+l_o region. This result is in contrast to the gradual decrease in the lateral diffusion rates observed between 2.5 and 20 mol% Chol reported by Filippov and coworkers [14,15]. The invariance of the ^{31}P MAS NMR line width to changing Chol concentration above T_m is most likely the result of timescale differences, with the line width timescale being much shorter than the lateral diffusion process.

The most notable item in the ^{31}P MAS NMR line width variation is the pronounced effect that cholesterol has on the appearance of the gel phase pretransition (Fig. 2). Inclusion of <10 mol% cholesterol diminishes this pretransition, and for Chol concentrations >10 mol%, the gel phase pretransition is completely eliminated. Several explanations have been forwarded to explain this observed ^{31}P MAS NMR line width variation in the gel phase, including the presence of a distinct gel → gel phase transition, dynamical changes in the bilayer, and changes in headgroup motional correlation times. These possibilities will be addressed in the following sections.

3.2. Differential scanning calorimetry

One possible explanation for the observed gel phase ^{31}P MAS NMR line width variation is a gel → gel transition, such as that observed in the gel phase to rippled phase [35] or the gel-α to gel-β transition [32]. Differential scanning calorimetry (DSC) was used to investigate a possible phase transition in the temperature region prior to the main gel to liquid crystalline transition. The calorimetric heating scans for SM and SM with 7.5 mol% Chol are displayed in Fig. 4. For SM, the endothermic gel → L_α phase transition is marked by a broad peak centered at 313.7 K (40.7 °C), while there is no visible indication of a pretransition (inset). The 7.5 mol% Chol bilayer also shows a broad main transition (313.1 K, 40.1 °C) with no measurable pretransition (inset). The main phase transition temperature for SM and the 0.6 °C shift to lower temperatures seen with the inclusion of Chol correlate well with previous reports [5,7,53–56]. Although pretransitions have been reported in the DSCs of SM, they have only been observable for synthetic and/or purified SM, with pretransition temperatures at approximately 301 K for purified 16:0-SM [7,31,36,37], from 293 K to 309 K for synthetic 18:0-SM (depending upon hydration) [32,57], and ~312 K for 24:0-SM [6,10,36]. The lack of an observable pretransition in the DSC shown here suggests the pretransition observed in the ^{31}P MAS NMR line width data between 300 K and 310 K is not the result of a bulk gel → gel phase transition.

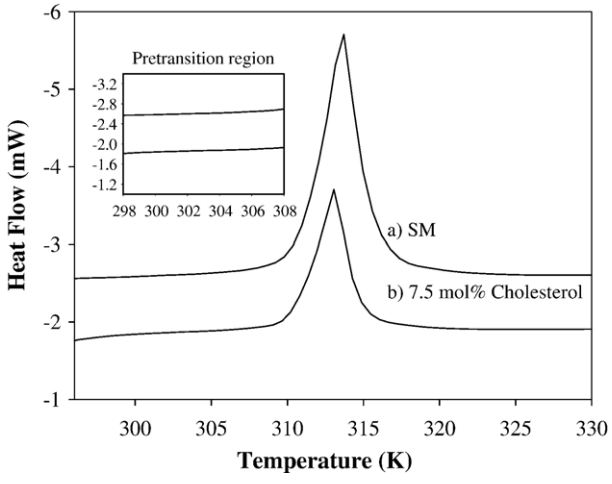

Fig. 4. DSC profiles of (a) SM and (b) SM with 7.5 mol% cholesterol. The pretransition temperature range is expanded in the inset.

3.3. Variation of ^{31}P MAS CSA with cholesterol concentration and temperature

A second argument is that the observed line width variation during this gel phase pretransition is the result of purely dynamical changes occurring on the ^{31}P CSA timescale. The variations of the CSA parameters from the ^{31}P MAS NMR spectra as a function of cholesterol concentration and temperature have therefore been explored. The ^{31}P MAS NMR CSA parameters for pure SM and SM with varying mol% of Chol are displayed in Fig. 5a while the temperature variation for these mixtures is shown in Fig. 5b. For samples with <33 mol% Chol there is a dramatic reduction in the ^{31}P CSA at T_m, and the production of a symmetric ^{31}P CSA tensor. This change is indicative of the main gel to L_α phase transition, and shows that there are headgroup motions on the order of a ~15 ppm (3600 Hz) leading to partial averaging of the ^{31}P CSA tensor.

Below the main gel to L_α phase transition the 0 mol% Chol (pure SM) sample has ^{31}P CSA value of $\Delta\sigma$=56.8 ppm (296 K) and corresponds to the gel (s_o) phase. The ^{31}P CSA anisotropy decreases to $\Delta\sigma$=55.6 ppm with the addition of 5 mol% Chol.

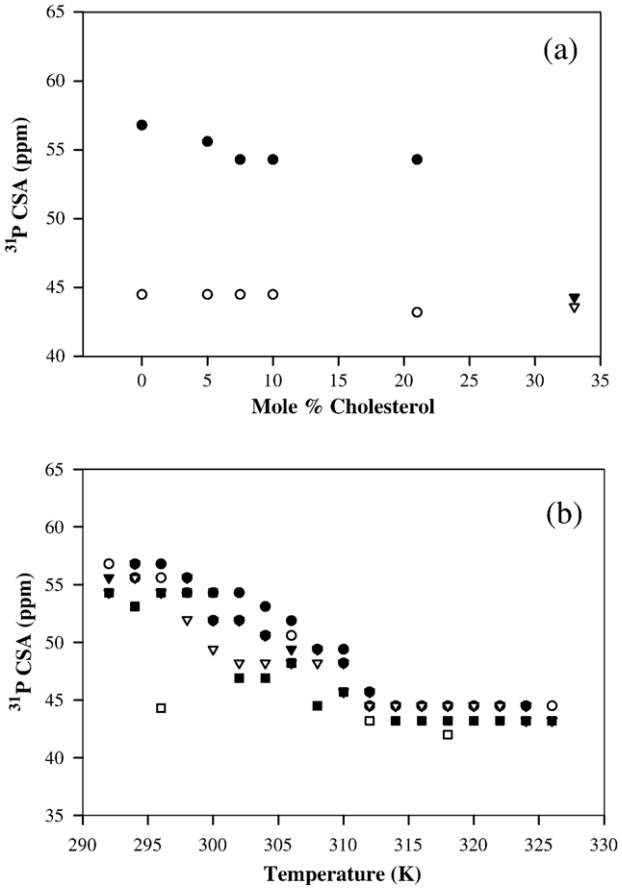

Fig. 5. (a) The ^{31}P CSA ($\Delta\sigma$) parameters extracted from ^{31}P MAS NMR fits of the spinning sideband manifold at (●) 296 K and (○) 318 K as a function of Chol concentration. SM and 33 mol% Chol at (▼) 296 K and (▽) 318 K from previous studies are also shown [48]. (b) The ^{31}P CSA parameters as a function of temperature for (●) SM, (○) 5 mol% Chol, (▼) 7.5 mol% Chol, (▽) 10 mol% Chol, and (■) 21 mol% Chol. SM and 33 mol% Chol (□) is shown at select temperatures for comparison and is from a previous work [48].

The CSA again decreases for the 7.5 mol% Chol mixture ($\Delta\sigma$= 54.3 ppm) and remains at the same value for bilayers containing 10 and 21 mol% Chol. Only at 33 mol% Chol is an additional ~10 ppm decrease in CSA observed with $\Delta\sigma$=44.3 ppm (296 K), which corresponds to the l_o phase. In the intermediate Chol concentration range no distinct ^{31}P NMR spectral signature for the co-existing s_o+l_o phase was observed. The decrease in the ^{31}P CSA with the addition of Chol is consistent with the averaging between the two phases, with increasing l_o concentration at higher Chol content. Analysis of this ^{31}P CSA trend is complicated by the presence of multi-component gel (s_o) phase ^{31}P NMR spectra [48], and variation in the degree of magnetic alignment. A detailed discussion on the ^{31}P NMR CSA variation will be presented in a future publication.

Above T_m the ^{31}P CSA shows only a minor variation ranging from $\Delta\sigma$=44.5 ppm (318 K) for the l_d phase (0 mol% Chol) to $\Delta\sigma$=43.6 ppm (318 K) for the l_o phase (33 mol% Chol). These results support the argument that the SM headgroup dynamics are very similar for the concentration range of Chol studied. The invariance of the ^{31}P CSA to the two-phase (l_d+l_o) regions most likely results from the rapid exchange of lipid between the l_o and l_d phases on the timescale of hundred of microseconds, suggesting very small domain sizes (~10 nm) as previously discussed [48], or that the ordering of the acyl chains in the l_o phase has a minimal impact on the dynamics detectable through measurement of the ^{31}P CSA tensor.

The overall decrease in ^{31}P CSA with increasing temperature in the gel phase does not correlate with the increasing ^{31}P MAS NMR line width shown in Fig. 2, since the predicted increase in headgroup dynamics should narrow the ^{31}P isotropic line width in this region. Because this predicted trend was not observed in the FWHM data, the observed gel phase pretransition is not being attributed to a purely dynamical change on a timescale measurable by the ^{31}P CSA (~12 kHz). It has been suggested that the ^{31}P CSA reduction results purely from a change in the headgroup orientation near T_m, such that the increasing ^{31}P MAS NMR line width in the gel pretransition reflects an increase in the heterogeneity of this orientation. The observation of a symmetric ^{31}P CSA tensor above T_m and an asymmetric tensor below T_m argues against the CSA reduction occurring entirely from a change in headgroup orientation.

3.4. Variation of ^{31}P NMR T_2 with cholesterol concentration and temperature

Spin–spin (T_2) relaxation measurements were also performed to complement the ^{31}P CSA results. The ^{31}P T_2 relaxation times are sensitive to molecular processes with correlation times equal to the inverse chemical shift anisotropy determined from the width of the SSB pattern (Fig. 1a, $\Delta\sigma$ ~80 ppm or ~20 kHz) [58]. The results of the ^{31}P T_2 relaxation measurements as a function of temperature are displayed in Fig. 6. Below T_m, the T_2 relaxation times are similar for pure SM, 5 mol% Chol, and 7.5 mol% Chol mixtures (1–2 ms), consistent with a dynamically restricted headgroup. At the main phase transition temperature, a sharp increase in T_2 is seen for SM bilayers with less than 10 mol% Chol and the L_α phase is marked by values ranging

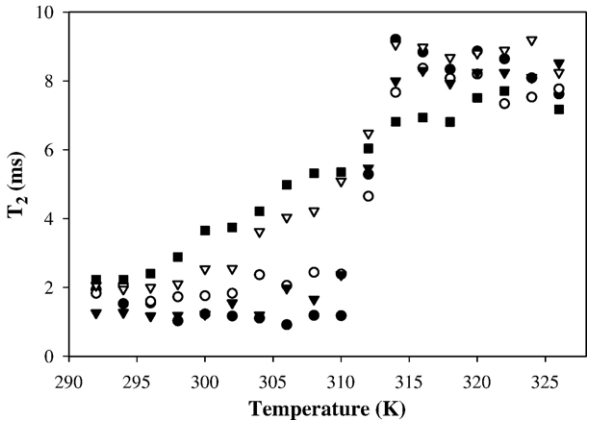

Fig. 6. ^{31}P MAS NMR T_2 relaxation times as a function of temperature for (●) SM, (○) 5 mol% Chol, (▼) 7.5 mol% Chol, (▽) 10 mol% Chol, and (■) 21 mol % Chol.

from 8 to 10 ms, indicating a dynamically mobile phase. For >10 mol% Chol the T_2 measurements display a gradual increase with higher temperatures, throughout the gel (s_o) phase and into the L_α (or l_d) phase. For the higher Chol concentrations the main phase transition is not clearly distinguishable with the T_2 measurements, similar to the ^{31}P MAS NMR line width measurements. The increasing T_2 values correlate well with the decreasing FWHM values for SM bilayers with >10% Chol, indicating an increase in the motional processes of the phosphorous headgroup and a reduction in the correlation time governing T_2. The similarity of ^{31}P T_2 relaxation times for intermediate Chol content also shows that these relaxation measurements are not sensitive to the presence of the two-phase s_o+l_o or the l_d+l_o regions. The ^{31}P NMR T_2 measurements are also in agreement with the ^{31}P CSA observations, revealing no pretransition in the gel phase for SM with Chol concentrations <10 mol%. These results support the conclusion that the molecular motions measurable by the ^{31}P T_2 and CSA (12–20 kHz) are not responsible for the ^{31}P MAS NMR line width gel phase pretransition observed in the FWHM data.

3.5. Impact of proton decoupling, field strength, and sample spin rate on line width broadening

The ^{31}P CSA is the dominant nuclear interaction for ^{31}P at high frequencies [59], and therefore the ^{31}P MAS NMR spectra reported here were collected without ^{1}H decoupling at 14.1 T. However, due to the unusual increase in line width, the effects of heteronuclear ^{1}H–^{31}P dipolar coupling, magnetic field strength, and sample spin rate were also explored in an effort to explain the observed gel phase pretransition. Previously, Holland et al. [48] showed that residual ^{1}H–^{31}P dipolar coupling was still present under ^{31}P MAS conditions at a spinning speed of 2 kHz, while in the L_α (or l_d) phase, the heteronuclear dipolar coupling was averaged out. A similar effect can be seen in Fig. 7a, where a narrowing of ~113 Hz is seen in the ^{31}P MAS NMR line width of SM (0 mol% Chol) at 296 K with the addition of ^{1}H decoupling. Despite this narrowing, the overall change in ^{31}P MAS NMR line width during the pretransition range is the same with and without ^{1}H decoupling supporting the argument that ^{1}H–^{31}P dipolar interactions are not responsible for the observed line width variations.

The impact of magnetic field strength on ^{31}P MAS line width is shown in Fig. 7a. These experiments show that the gel phase pretransition is essentially unaffected by changes in the magnetic field, with the overall change in ^{31}P line width (ΔFWHM) in the same temperature range (296 K–310 K) revealing similar values for SM at 9.4 T (140 Hz) and SM at 14.1 T (173 Hz). The dramatic decrease in line width marking the main transition at both fields is also approximately the same (320 Hz at 9.4 T compared to 380 Hz at 14.1 T). In the L_α (or l_d) phase, however, the 9.4 T line widths are slightly narrower (~50 Hz) than the line widths seen at higher field, partially due to the difference in the field homogeneity and quality of shimming with a different magnet. Spin–spin T_2 relaxation measurements were also conducted at a lower magnetic field (data not shown) and did not reveal any correlated change in T_2 values. These results suggest that the observed ^{31}P MAS NMR line width variation in the gel phase pretransition is not directly tied to the magnitude of the ^{31}P CSA.

It has also been suggested that the increase in line width observed in the gel phase pretransition arises from destructive

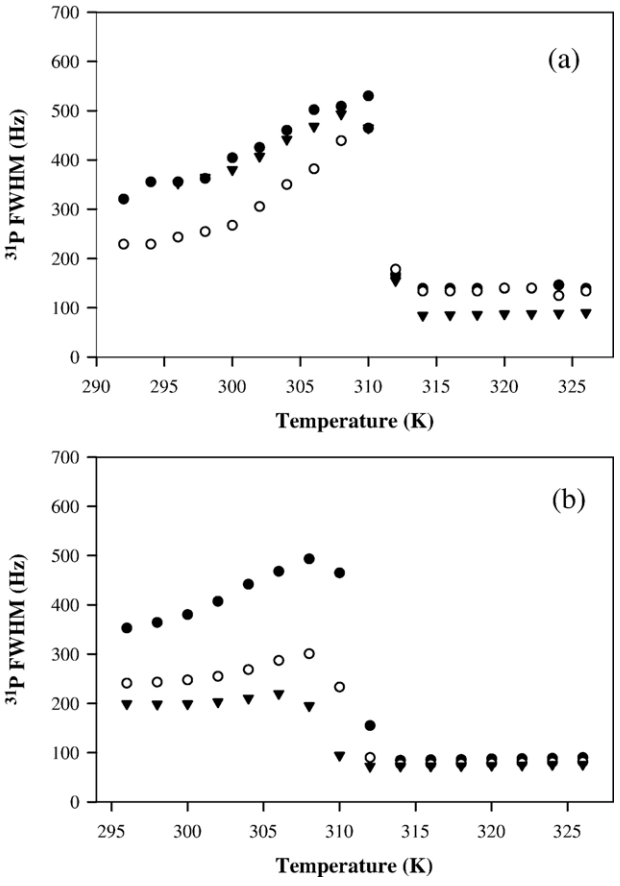

Fig. 7. (a) The ^{31}P MAS NMR isotropic full width at half maximum (FWHM) line width as a function of temperature for (●) SM at 14.1 T, (○) SM with ^{1}H decoupling at 14.1 T and (▼) SM at 9.4 T. (b) The ^{31}P isotropic full width at half maximum (FWHM) line width for SM at 9.4 T as a function of temperature and rotor frequency at (●) ν_r=2 kHz, (○)ν_r=4 kHz, and (▼)ν_r=6 kHz.

interference between the coherent averaging of MAS and incoherent molecular averaging processes [60,61]. To address this possibility, the ^{31}P MAS NMR line width was measured at different spinning speeds at 9.4 T (Fig. 7b). Increasing the sample spinning speed from 2 kHz to 4 kHz and finally 6 kHz dampens the observed gel phase pretransition, with a reduction in the ^{31}P MAS NMR line width variation of 60 Hz (ν_r=4 kHz) and 80 Hz (ν_r=6 kHz). Temperature effects due to frictional spinning under MAS have been accounted for, and result in a shift of the pretransition, not a dampening of the transition with increasing spin rate. This result shows that the gel phase pretransition observed in the ^{31}P MAS line width variation results from slow headgroup motions with correlation times on the order of 2 to 6×10^{-5} s ($\tau_c \sim 0.7/\omega_r$, where ω_r is the MAS rotor frequency in rad/s) [61]. This is a slightly slower timescale than measured by the ^{31}P T_2 relaxation and CSA studies, which showed no clear evidence of a pretransition. The addition of Chol increases the rate of the headgroup motions reducing the interference with the coherent averaging of the MAS.

One final possibility for this observed gel phase pretransition in SM is a subtle change in the local headgroup structural environments (leading to a distribution of chemical shifts) just prior to the gel → L_α phase transition that is eliminated with the addition of cholesterol. Compared to other lipids with a glycerol backbone, SM has been shown to have unique intra- and intermolecular hydrogen bonding properties due the hydroxyl and amide groups on the sphingosine backbone [42–44,62], that may be disrupted by the addition of Chol. The SM headgroup may undergo significant structural changes during the gel → L_α transition with the ^{31}P MAS NMR line width variations reflecting SM preparing for this transition. With increasing Chol content, these intra- and intermolecular bonding interactions are reduced, and correspondingly the required structural changes in SM diminished. On the other hand this increased distribution of ^{31}P NMR chemical shifts should not be influenced by the variation in spinning speed as was observed experimentally.

4. Conclusions

The ^{31}P MAS NMR spectra for SM and SM with 5, 7.5, 10, and 21 mol% Chol have been presented. The variations in ^{31}P MAS NMR line width indicate a transition is occurring in the gel phase prior to the main gel → L_α. The incorporation of Chol into the bilayer diminishes this gel phase transition. Possible explanations for this observation included a gel → gel phase transition, dynamical changes, and changes in correlation times. The DSC results show it is not a bulk gel → gel transition. Analysis of the ^{31}P NMR data shows that it does not result from CSA, ^{1}H–^{31}P dipolar coupling or T_2 relaxation effects. The observed pretransition appears to be due to slow motions on the order of the MAS spinning speed or a result of a local disorder in the headgroup region, possibly due to changes in intramolecular and/or intermolecular hydrogen bonding. Although subtle, these changes are readily apparent in the ^{31}P MAS NMR as an increase in line width that is diminished with the addition of 10 mol% cholesterol. The results demonstrate how low concentrations of cholesterol can have an impact on the headgroup structure/dynamics of sphingomyelin, further illustrating the complexity of the sphingomyelin in membrane systems.

Acknowledgements

This work was supported by the Sandia Laboratory Directed Research Development program. Sandia is a multiprogram laboratory operated by Sandia Corporation, a Lockheed Martin company, for the United States Department of Energy's National Nuclear Security Administration under contract DE-AC04-94AL85000. The authors would like to acknowledge Ryan S. Berry and Mark E. Stavig for performing the differential scanning calorimetry measurements.

References

[1] K. Simons, E. Ikonen, Functional rafts in cell membranes, Nature 387 (1997) 569–572.
[2] D.A. Brown, E. London, Structure and function of sphingolipid- and cholesterol-rich membrane rafts, J. Biol. Chem. 275 (2000) 17221–17224.
[3] K. Simons, W.L.C. Vaz, Model systems, lipid rafts, and cell membranes, Annu. Rev. Biophys. Biomol. Struct. 33 (2004) 269–295.
[4] F.G. van der Goot, T. Harder, Raft membrane domains: from a liquid-ordered membrane phase to a site of pathogen attack, Semin. Immunol. 13 (2001) 89–97.
[5] P.R. Maulik, G.G. Shipley, N-palmitoyl sphingomyelin bilayers: structure and interactions with cholesterol and dipalmitoylphosphatidylcholine, Biochemistry 35 (1996) 8025–8034.
[6] T.J. McIntosh, S.A. Simon, D. Needham, C. Huang, Structure and cohesive properties of sphingomyelin/cholesterol bilayers, Biochemistry 31 (1992) 2012–2020.
[7] T.K.M. Nyholm, M. Nylund, J.P. Slotte, A calorimetric study of binary mixtures of dihydrosphingomyelin and sterols, sphingomyelin, or phosphatidylcholine, Biophys. J. 84 (2003) 3138–3146.
[8] T. Rog, M. Pasenkiewica-Gierula, Cholesterol–sphingomyelin interactions: a molecular dynamics simulation study, Biophys. J. 91 (2006) 3756–3767.
[9] G.A. Khelashvilli, H.L. Scott, Combined Monte Carlo and molecular dynamics simulation of hydrated 18:0 sphingomyelin–cholesterol lipid bilayers, J. Chem. Phys. 120 (2004) 9841–9847.
[10] P.R. Maulik, G.G. Shipley, X-ray diffraction and calorimetric study of N-lignoceryl sphingomyelin membranes, Biophys. J. 69 (1995) 1909–1916.
[11] R.F.M. de Almeida, A. Fedorov, M. Prieto, Sphingomyelin/Phosphatidylcholine/Cholesterol phase diagram: boundaries and composition of lipid rafts, Biophys. J. 85 (2003) 2406–2416.
[12] M.B. Sankaram, T.E. Thompson, Interaction of cholesterol with various glycerophospholipids and sphingomyelin, Biochemistry 29 (1990) 10670–10675.
[13] A. Filippov, G. Oradd, G. Lindblom, The effect of cholesterol on the lateral diffusion of phospholipids in oriented bilayers, Biophys. J. 84 (2003) 3079–3086.
[14] A. Filippov, G. Oradd, G. Lindblom, Lipid lateral diffusion in ordered and disordered phases in raft mixtures, Biophys. J. 86 (2004) 891–896.
[15] A. Filippov, G. Oradd, G. Lindblom, Sphingomyelin structure influences the lateral diffusion and raft formation in lipid bilayers, Biophys. J. 90 (2006) 2086–2092.
[16] R.A. Demel, J.W.C.M. Jansen, P.W.M. van Dijck, L.L.M. van Deenen, The preferential interaction of cholesterol with different classes of phospholipids, Biochim. Biophys. Acta 465 (1977) 1–10.
[17] B. Ramstedt, J.P. Slotte, Interaction of cholesterol with sphingomyelins and acyl-chain-matched phosphatidylcholines: a comparative study of the effect of the chain length, Biophys. J. 76 (1999) 908–915.
[18] S. Niu, B.J. Litman, Determination of membrane cholesterol partition coefficient using a lipid vesicle-cyclodextrin binary system: effect of

phospholipid acyl chain unsaturation and headgroup composition, Biophys. J. 83 (2002) 3408–3415.
[19] B. Terova, R. Heczko, J.P. Slotte, On the importance of the phosphocholine methyl groups for sphingomyelin/cholesterol interactions in membranes: a study with ceramide phosphoethanolamine, Biophys. J. 88 (2005) 2661–2669.
[20] W. Guo, V. Kurze, T. Huber, N.H. Afdhal, K. Beyer, J.A. Hamilton, A solid-state NMR study of phospholipid–cholesterol interactions: sphingomyelin–cholesterol binary systems, Biophys. J. 83 (2002) 1465–1478.
[21] J.R. Silvius, Role of cholesterol in lipid raft formation: lessons from lipid model systems, Biochim. Biophys. Acta 1610 (2003) 174–183.
[22] P.W.M. van Dijck, B. de Kruijff, L.L.M. van Deenen, J. de Geir, R.A. Demel, The preference of cholesterol for phosphatidylcholine in mixed phosphatidylcholine–phosphatidylethanolamine bilayers, Biochim. Biophys. Acta 455 (1976) 576–587.
[23] P.L. Yeagle, J.E. Young, Factors contributing to the distribution of cholesterol among phospholipid vesicles, J. Biol. Chem. 261 (1986) 8175–8181.
[24] B. Ramstedt, J.P. Slotte, Sphingolipids and the formation of sterol-enriched ordered membrane domains, Biochim. Biophys. Acta 1758 (2006) 1945–1956.
[25] J.B. Huang, J.T., G.W. Feigenson, Maximum solubility of cholesterol in phosphatidylcholine and phosphatidylethanolamine bilayers, Biochim. Biophys. Acta 1417 (1999) 89–100.
[26] C. Kan, Z. Ruan, R. Bittman, Interaction of cholesterol with sphingomyelin in bilayer membranes: evidence that the hydroxy group of sphingomyelin does not modulate the rate of cholesterol exchange between vesicles, Biochemistry 30 (1991) 7759–7766.
[27] R. Bittman, C.R. Kasireddy, P. Mattjus, J.P. Slotte, Interaction of cholesterol with sphingomyelin in monolayers and vesicles, Biochemistry 33 (1994) 11776–11781.
[28] M.P. Veiga, J.L.R. Arrondo, F.M. Goni, A. Alonso, D. Marsh, Interaction of cholesterol with sphingomyelin in mixed membranes containing phosphatidylcholine, studied by spin-label ESR and IR spectroscopies. A possible stabilization of gel-phase sphingolipid domains by cholesterol, Biochemistry 40 (2001) 2614–2622.
[29] T. Heimburg, A model for the lipid pretransition: coupling of ripple formation with the chain-melting transition, Biophys. J. 78 (2000) 1154–1165.
[30] M. Kranenburg, B. Smit, Phase behavior of model lipid bilayers, J. Phys. Chem., B 109 (2005) 6553–6563.
[31] B. Ramstedt, J.P. Slotte, Comparison of the biophysical properties of racemic and D-erythro-*N*-acyl sphingomyelins, Biophys. J. 77 (1999) 1498–1506.
[32] K.S. Bruzik, M. Tsai, A calorimetric study of the thermotropic behavior of pure sphingomyelin diastereomers, Biochemistry 26 (1987) 5364–5368.
[33] Y. Barenholz, J. Suurkuusk, D. Mountcastle, T.E. Thompson, R.L. Biltonen, A calorimetric study of the thermotropic behavior of aqueous dispersions of natural and synthetic sphingomyelins, Biochemistry 15 (1976) 2441–2447.
[34] R. Cohen, y. Barenholz, S. Gatt, A. Dagan, Preparation and characterization of well defined D-erythro sphingomyelins, Chem. Phys. Lipids 35 (1984) 371–384.
[35] H.W. Meyer, H. Bunjes, A.S. Ulrich, Morphological transitions of brain sphingomyelin are determined by the hydration protocol: ripples re-arrange in plane, and sponge-like networks disintegrate into small vesicles, Chem. Phys. Lipids 99 (1999) 111–123.
[36] L.K. Bar, Y. Barenholz, T.E. Thompson, Effect of sphingomyelin composition on the phase structure of phosphatidylcholine–sphingomyelin bilayers, Biochemistry 36 (1997) 2507–2516.
[37] M. Kuikka, B. Ramstedt, H. Ohvo-Rekila, J. Tuuf, J.P. Slotte, Membrane properties of D-erythro-*N*-acyl sphingomyelins and their corresponding dihyro species, Biophys. J. 80 (2001) 2327–2337.
[38] R.M. Epand, Cholesterol in bilayers of sphingomyelin or dihydrosphingomyelin at concentrations found in ocular lens membranes, Biophys. J. 84 (2003) 3102–3110.
[39] S.W. Hui, T.P. Stewart, P.L. Yeagle, Temperature-dependent morphological and phase behavior of sphingomyelin, Biochim. Biophys. Acta 601 (1980) 271–281.
[40] C. Chachaty, D. Rainteau, C. Tessier, P.J. Quinn, C. Wolf, Building up of the liquid-ordered phase formed by sphingomyelin and cholesterol, Biophys. J. 88 (2005) 4032–4044.
[41] P.R. Cullis, M.J. Hope, The bilayer stabilizing role of sphingomyelin in the presence of cholesterol, Biochim. Biophys. Acta 597 (1980) 533–542.
[42] C.F. Schmidt, Y. Barenholz, T.E. Thompson, A nuclear magnetic resonance study of sphingomyelin in bilayer systems, Biochemistry 16 (1977) 2649–2656.
[43] I.C. Malcolm, J.C. Ross, J. Higinbotham, A study of the headgroup motion of sphingomyelin using ^{31}P NMR and an analytically soluble model, Solid State Nucl. Magn. Reson. 27 (2005) 247–256.
[44] E. Mombelli, R. Morris, W. Taylor, F. Fraternali, Hydrogen-bonding propensities of sphingomyelin in solution and in a bilayer assembly: a molecular dynamics study, Biophys. J. 84 (2003) 1507–1517.
[45] P. Niemela, M.T. Hyvonen, I. Vattulainen, Structure and dynamics of sphingomyelin bilayer: insight gained through systematic comparison to phosphatidylcholine, Biophys. J. 87 (2004) 2976–2989.
[46] S.W. Chiu, S. Vasudevan, E. Jakobsson, R.J. Mashl, H.L. Scott, Structure of sphingomyelin bilayers: a simulation study, Biophys. J. 85 (2003) 3624–3635.
[47] F. Aussenac, M. Tavares, E.J. Dufourc, Cholesterol dynamics in membranes of raft composition: a molecular view from ^{2}H and ^{31}P solid-state NMR, Biochemistry 42 (2003) 1383–1390.
[48] G.P. Holland, S.K. McIntyre, T.M. Alam, Distinguishing individual lipid headgroup mobility and phase transitions in raft-forming lipid mixtures with ^{31}P MAS NMR, Biophys. J. 90 (2006) 4248–4260.
[49] K.S. Bruzik, B. Sobon, G.M. Salamonczyk, Nuclear magnetic resonance study of sphingomyelin bilayers, Biochemistry 29 (1990) 4017–4021.
[50] T.M. Alam, G.P. Holland, ^{1}H–^{13}C INEPT MAS NMR correlation experiments with ^{1}H–^{1}H mediated magnetization exchange to probe organization in lipid biomembranes, J. Magn. Res. 180 (2006) 210–221.
[51] D. Massiot, F. Fayon, M. Capron, I. King, S. Le Calve, B. Alonso, J.-O. Durand, B. Bujoli, Z. Gan, G. Hoatson, Modeling one- and two-dimensional solid-state NMR spectra, Magn. Reson. Chem. 40 (2002) 70–76.
[52] J. Seelig, ^{31}P nuclear magnetic resonance and the head group structure of phospholipids in membranes, Biochim. Biophys. Acta 515 (1978) 105–140.
[53] M.B. Ruiz-Arguello, M.P. Veiga, J.L.R. Arrondo, F.M. Goni, A. Alonso, Sphingomyelinase cleavage of sphingomyelin in pure and mixed lipid membranes. Influence of the physical state of the sphingolipid, Chem. Phys. Lipids 114 (2002) 11–20.
[54] W.I. Calhoun, G.G. Shipley, Sphingomyelin–lecithin bilayers and their interaction with cholesterol, Biochemistry 18 (1979) 1717–1722.
[55] P.R. Maulik, G.G. Shipley, Interactions of N-stearoyl sphingomyelin with cholesterol and dipalmitoylphosphatidylcholine in bilayer membranes, Biophys. J. 70 (1996) 2256–2265.
[56] D.A. Mannock, T.J. McIntosh, X. Jiang, D.F. Covey, R.N. McElhaney, Effects of natural and enantiomeric cholesterol on the thermotropic phase behavior and structure of egg sphingomyelin bilayer membranes, Biophys. J. 84 (2003) 1038–1046.
[57] P.R. Maulik, P.K. Sripada, G.G. Shipley, Structure and thermotropic properties of hydrated N-stearoyl sphingomyelin bilayer membranes, Biochim. Biophys. Acta 1062 (1991) 211–219.
[58] E.J. Dufourc, C. Mayer, J. Stohrer, G. Althoff, G. Kothe, Dynamics of phosphate head groups in biomembranes: comprehensive analysis using phosphorus-31 nuclear magnetic resonance lineshape and relaxation time measurements, Biophys. J. 61 (1992) 42–57.
[59] M.P. Milburn, K.R. Jeffrey, Dynamics of the phosphate group in phospholipid bilayers, Biophys. J. 52 (1987) 791–799.
[60] N.L. Adolphi, S. Badola, L.A. Browder, J. Bowman, R.C., Magic-angle spinning NMR study of deuterium site occupancy and dynamics in $ZrNiD_{1.0}$ and $ZrNiD_{3.0}$, Phys. Rev., B 65 (2001) (024301-024301-024301-024309).
[61] D. Suwelack, W.P. Rothwell, J.S. Waugh, Slow molecular motion detected in the NMR spectra of rotating solids, J. Chem. Phys. 73 (1980) 2559–2569.
[62] K.S. Bruzik, Conformation of the polar headgroup of sphingomyelin and its analogues, Biochim. Biophys. Acta 939 (1988) 315–326.